Enhancing glioma-specific drug delivery through self-assembly of macrophage membrane and targeted polymer assisted by low-frequency ultrasound irradiation

Junqing Lin [a], Zhenhu Lin [b], Leilei Liu [c], Wenjin Lin [b], Xiaodong Xie [d,*], Xiujuan Zhang [b,**]

[a] Department of Interventional Radiology, Fujian Medical University Union Hospital, Fuzhou, China
[b] Department of Ultrasound, Fujian Medical University Union Hospital, Fuzhou, 350001, Fujian, China
[c] Department of Ultrasound, The Second Affiliated Hospital of Fujian Traditional Chinese Medical University, Fuzhou, 350001, Fujian, China
[d] Fujian-Taiwan-Hongkong-Macao Science and Technology Cooperation Base of Intelligent Pharmaceutics, College of Materials and Chemical Engineering, Minjiang University, Fuzhou, 350001, Fujian, China

ARTICLE INFO

ABSTRACT

The blood-brain Barrier (BBB), combined with immune clearance, contributes to the low efficacy of drug delivery and suboptimal treatment outcomes in glioma. Here, we propose a novel approach that combines the self-assembly of mouse bone marrow-derived macrophage membrane with a targeted positive charge polymer (An-PEI), along with low-frequency ultrasound (LFU) irradiation, to achieve efficient and safe therapy for glioma. Our findings demonstrate the efficacy of a charge-induced self-assembly strategy, resulting in a stable co-delivery nanosystem with a high drug loading efficiency of 44.2 %. Moreover, this structure triggers a significant release of temozolomide in the acidic environment of the tumor microenvironment. Additionally, the macrophage membrane coating expresses Spyproteins, which increase the amount of An-BMP-TMZ that can evade the immune system by 40 %, while LFU irradiation treatment facilitates the opening of the BBB, allowing for enormously increased entry of An-BMP-TMZ (approximately 400 %) into the brain. Furthermore, after crossing the BBB, the Angiopep-2 peptide-modified An-BMP-TMZ exhibits the ability to selectively target glioma cells. These advantages result in an obvious tumor inhibition effect in animal experiments and significantly improve the survival of glioma-bearing mice. These results suggest that combining the macrophage membrane-coated drug delivery system with LFU irradiation offers a feasible approach for the accurate, efficient and safe treatment of brain disease.

1. Introduction

Glioma is a primary brain tumor associated with poor prognosis and high mortality rates [1,2]. The treatment of glioma is a complicated yet extensively studied problem. Insufficient toxicity fails to eliminate cancer cells, while excessive toxicity can cause irreversible damage to brain tissue [3]. Therefore, targeted drug delivery has gained recognition among researchers as a means to improve therapeutic efficacy and reduce the risk of toxic and side effects [4–6]. The blood-brain barrier (BBB) is an endothelial membrane sheathed by parietal vascular cells and perivascular astrocyte end-feet that protect the brain from exogenous substance invasion [7]. Thus, many chemical drugs and targeted drug delivery systems cannot reach glioma due to the BBB, substantially

limiting the therapeutic effect of targeted drug delivery [8]. Previous studies have revealed that low-frequency ultrasound (LFU) irradiation at appropriate intensity levels can non-invasively, safely and reversibly open the BBB [9–11], rendering it possible for therapeutic drugs to reach brain tumors.

Currently, temozolomide (TMZ) is the sole available frontline DNA methylating adjuvant chemotherapy prodrug and the only FDA-approved first-line chemical drug for treating glioma [12–14]. The administration of TMZ has considerably improved the survival rate of glioma patients. However, direct use of TMZ has been frequently impeded by adverse events, including fatigue, nausea and cytopenia [15, 16]. Fortunately, recent studies have demonstrated that nano-based drug delivery systems (DDS) not only enhance the pharmacokinetics

---

of TMZ but also improve its efficacy in glioma treatment [13]. Moreover, using targeted DDS would significantly reduce the systemic side effects caused by TMZ's toxicity [17,18].

Targeted drug delivery using nano-sized biomaterials has significantly improved cancer treatment [19–21]. Previous studies have demonstrated that nano-sized biomaterials can target tumors through the enhanced permeability and retention (EPR) effect [22,23]. In recent years, cell membrane-coated nanoparticles (CNPs) have emerged as a promising avenue for the diagnosis, treatment, and prevention of disease [24]. By enveloping synthetic nanoparticulate cores with natural cell membranes, CNPs exhibit a diverse array of surface markers that enable them to replicate natural cellular interactions and find utility in a variety

of biomedical applications [25,26]. The specific markers on natural membrane-modified DDS integrate the physical and chemical properties of cells, which contribute to immune escape, long circulation, and low toxicity [27–29]. Among them, macrophage membrane has received exceptional attention owing to the abundant "spyproteins" and spontaneous targeting ability to tumor cells [30]. Furthermore, macrophage membrane shows high expression of CD47, which signals "don't eat me," leading to DDS resistance to phagocytosis by monocytes and macrophages [31,32]. Moreover, the integrin Lymphocyte Function-Associated Antigen 1 (LFA-1) expressed on macrophages is involved in the diapause of macrophages as they cross the endothelial barrier. This mechanism facilitates the delivery of cargo by drug
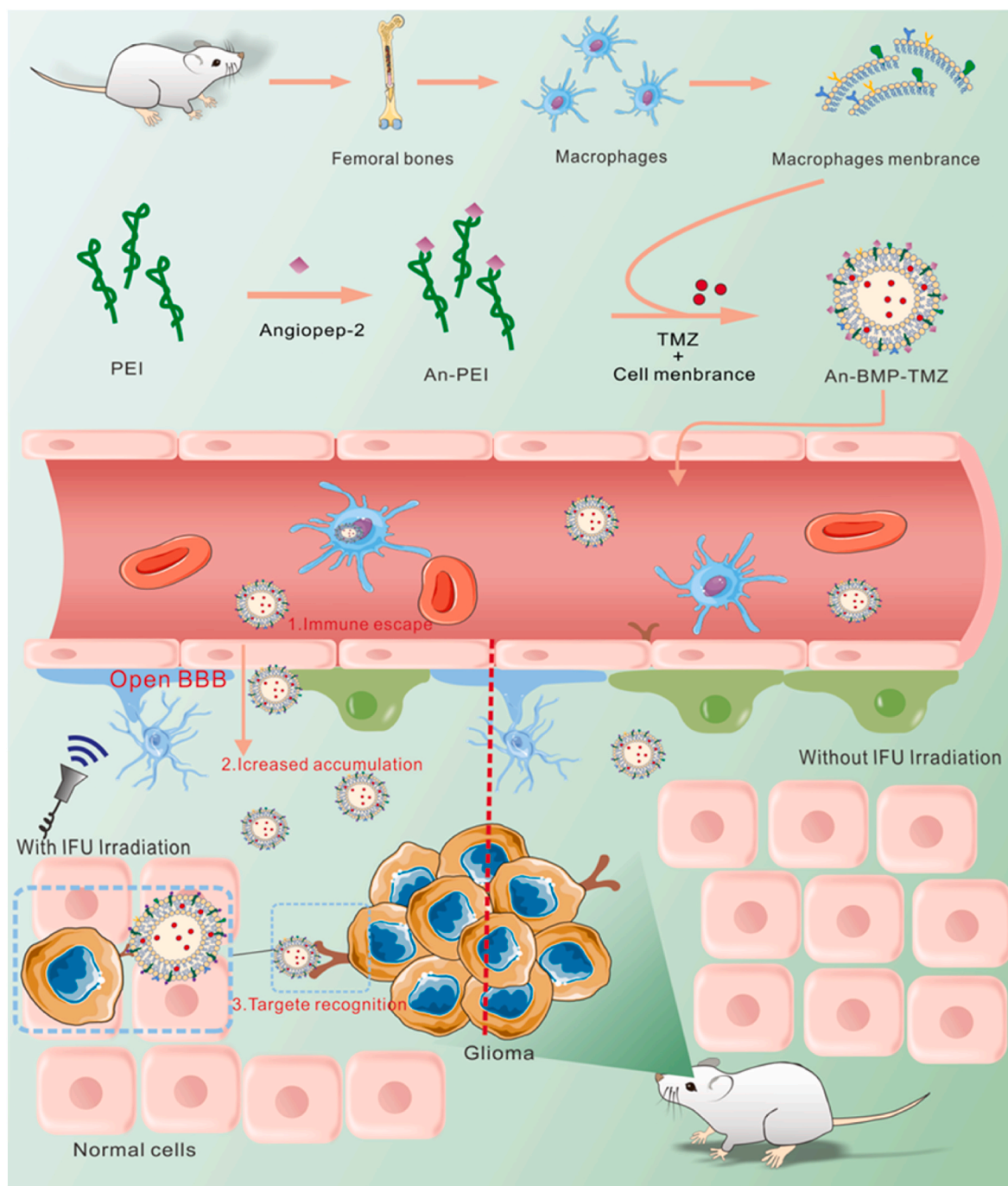

Fig. 1. Schematic illustration of the design of An-BMP-TMZ, and its mechanism of escaping the immune system and crossing the blood-brain barrier to reach glioma cells.

delivery systems to glioma cells within the brain [33].

Here we propose that the self-assembly of Angiopep-2 modified polyethyleneimine (PEI) with the mouse bone marrow-derived macrophage membrane, loaded with TMZ (An-BMP-TMZ), along with LFU irradiation could be used for efficient drug delivery to glioma (Fig. 1). Although some studies have employed LFU combined with nanocarriers for drug delivery across the BBB, most of these investigations have neglected the impact of immune cells in the circulatory system on the clearance of nanocarriers. In addition, the potential toxicity of nanocarriers to normal brain tissue after they crossing the BBB is often ignored [34–36]. In this investigation, the coating of the cell membrane on the nanoparticles' surfaces formed a diffusion barrier and limited the release of TMZ, and the release characteristics under acidic conditions potentially lead to enhancing the accumulation of TMZ in tumors and minimizing its impact on normal tissues. Proteins such as CD47 and LFA-1, which are present on the surface of An-BMP-TMZ, prolong the circulation of drug delivery systems. The treatment of LFU irradiation significantly enhances the accumulation of An-BMP-TMZ in the brain. The Angiopep-2 modification enables the specific delivery of TMZ to glioma, resulting in effectively suppressing primary brain tumor recurrence and prolonging overall survival *in vivo*. Moreover, An-BMP-TMZ demonstrates excellent safety attributed to their targeting ability and high biocompatibility derived from the coverage of mouse macrophage membrane, thereby avoiding toxic side effects. This macrophage membrane-coated targeted polymer combined with LFU irradiation may represent a suitable strategy for accurate, efficient and safe therapy of glioma.

2. Material and methods

2.1. Materials

Polyethyleneimine (PEI, 10 kDa) was obtained from Sigma. HOOC-PEG (2000)-Angiopep-2 was purchased from Guangzhou Carbon Water Technology Co., Ltd. Temozolomide was obtained from Aladdin Industrial Corporation. EDC and NHS were obtained from Aladdin Industrial Corporation. The primary anti-CD47 antibody and the secondary HRP Goat anti-rabbit IgG antibodies were obtained from ABclonal Technology Co., Ltd. The anti-EGFR antibody was obtained from abcam (ab214627). Fetal bovine serum (FBS) was purchased from Life Technologies. The Apoptosis Detection Kit was purchased from Genview. PKH26 and PKH67 were obtained from Umibio Science and Technology.

2.2. Cell culture

The U87 and U251 glioma cell lines were obtained from the Cell Bank of Shanghai, Chinese Academy of Sciences, while the bEnd3 cells were purchased from CytoBiotech (Shaanxi, China). Bone marrow-derived macrophages (BMDMs) were prepared from BALB/c mice using previously published methods [37]. Briefly, bone marrow was collected from the femoral bones of BALB/c mice, and the cells were isolated by centrifugation at 200*g* for 10 min. The cells were cultured in DMEM medium supplemented with 10 % FBS, 1 % penicillin/streptomycin, and macrophage colony-stimulating factor (50 ng/mL) from Biolegend. F4/80 antibody was used to characterize the BMDMs. The U87 and U251 cells were cultured in DMEM medium supplemented with 10 % fetal bovine serum and 1 % penicillin/streptomycin. All cells were maintained at 37 °C in a humidified incubator with 5 % CO_2.

2.3. Angiopep2 modified polyethylenimine

Ten mg of HOOC-PEG (2000)-Angiopep-2, 10 mg EDC and 8 mg NHS were dissolved in 5 mL of water and stirred for 15 min at 25 °C, followed by adding 10 mg of polyethylenimine (PEI, 10 kD). The excess EDC, NHS and unconjugated HOOC-PEG (2000)-Angiopep-2 were removed

through the ultrafiltration tube (5 kd) and the resulting product was resuspended in water.

2.4. Isolation of macrophage membrane

The bone marrow-derived macrophages (BMDMs) were harvested and incubated with ice-cold tris-magnesium buffer (TM-buffer, pH 7.4, 0.01 M Tris, and 0.001 M MgCl2). The mixture was centrifuged at 2000 g for 10 min, and the supernatant was collected and centrifuged at 15,000 g for 30 min to collect cell membrane. The cell membrane was sonicated at a frequency of 42 kHz and a power of 100 W for 10 min.

2.5. Preparation of TMZ loaded nanocarriers

To prepare BMDMs cell membrane-PEI nanoparticles, we mixed 10 mg of Temozolomide (TMZ) with either 10 mg of PEI or PEI-Angiopep2 and the cell membrane from 1×10^8 cells in water. The mixture was sonicated at a frequency of 42 kHz and a power of 100 W for 10 min, and then extruded through a mini-extruder (Avestin, LF-1, Canada) using a 200 nm polycarbonate membrane for at least 10 passes. Following extrusion, we collected the TMZ loaded nanoparticles via centrifugation at 15,000 g for 30 min. The amount of TMZ in An-BMP-TMZ was determined by subtracting the amount of TMZ in the supernatant from the total added drug amount [30]. The drug concentration in the supernate could be determined with absorbance measurement at 330 nm [38].

2.6. In vitro release of TMZ

The release of TMZ from An-BMP-TMZ was conducted in PBS (pH 7.4 and pH 5.5) at 37 °C. BMP-TMZ or An-BMP-TMZ (TMZ amount = 0.5 mg) was dissolved in 10 mL PBS at 37 °C and shaken at 100 rpm. The samples were collected at different time points, and the samples were centrifuged at 15,000 g for 30 min. The accumulated release of TMZ in the supernatant was calculated by absorbance measurement at 330 nm from the established standard curve using TECAN Infinite F200 Microplate Reader.

2.7. Characterization of an-BMP-TMZ

The size distribution and zeta potential of An-BMP-TMZ were measured with Malvern Instruments Zetasizer HS III (Malvern, UK). The shape and surface appearance of An-BMP-TMZ were determined with atomic force microscopy (AFM; Bruker Co., Germany) and Transmission Electron Microscopy (TEM; JEM-1400plus, Japan). The amount of conjugated HOOC-PEG (2000)-Angiopep-2 was calculated by using the amount of Angiopep-2 added minus the amount of unconjugated Angiopep-2. The amount of unconjugated HOOC-PEG (2000)-Angiopep-2 was measured with BCA kit and standard curve [39].

2.8. The expression of CD47 and LFA-1 on an-BMP-TMZ

The CD47 protein on the cell membrane serves as a crucial "don't eat me" signal to the innate immune system, preventing immune clearance of An-BMP-TMZ [32]. The LFA-1 expressed on macrophages is involved in the diapause of macrophages as they cross the endothelial barrier. In this study, the expressions of CD47 and LFA-1 on BMP-TMZ and An-BMP-TMZ were quantified using western blot analysis. In brief, BMP-TMZ and An-BMP-TMZ were incubated in RIPA lysis buffer with 1 % protease inhibitor and 1 % PMSF, followed by centrifugation (12,000 g) at 4 °C for 15 min to collect supernatants. Protein concentration was measured using the BCA method before electrophoresis. The membranes were then incubated with anti-CD47 primary antibodies (Rabbit anti mouse, ABclonal) or anti-LFA-1 primary antibodies (Rabbit anti mouse, ThermoFisher) for 1 h, washed three times with TBS-T, and incubated with secondary antibody. The results were visualized using the Bio-Rad

ChemiDoc MP system.

2.9. Stability of an-BMP-TMZ

An-BMP-TMZ was incubated in DMEM culture medium with 10 % FBS or mouse serum for 4 h, and the stability of the nanoparticles was determined with Malvern Instruments Zetasizer HS III (Malvern, UK). The results were determined with DLS [14].

2.10. In vitro cytotoxicity assay

To assess the *in vitro* cytotoxicity of An-BMP-TMZ against glioma cells, U87 and U251 glioma cell lines were seeded into 96-well plates at a density of 10,000 cells per well and incubated for 48 h at 37 °C with 5 % CO_2. Following this, the cells were treated with BMP-TMZ or An-BMP-TMZ at various TMZ concentrations (0.02, 0.05, 0.1, 0.2, 0.5, 1, 2, 4 mM) for another 48 h. After treatment, the medium was aspirated and cells were washed three times with PBS, followed by incubation with MTT for 4 h at 37 °C. The supernatant was removed, and 100 μL DMSO was added to each well. Absorbance of the solution was measured at 490 nm using a TECAN Infinite F200 Microplate Reader. To assess the cytotoxicity of the drug-free carrier, both modified (An-BMP) and un-modified (BMP) blank nanocarriers were subjected to an *in vitro* cytotoxicity assay. The assay employed identical PEI concentrations as those used in BMP-TMZ and An-BMP-TMZ formulations.

2.11. Nanoparticle labeling

To track the nanoparticles, the fluorescent dye PKH26 (λex = 551 nm and λem = 567 nm, Umibio) was used to label An-BMP-TMZ according to the instructions.

2.12. In vitro uptake of an-BMP-TMZ

To evaluate the specific uptake of An-BMP-TMZ by glioma cells, U87 and U251 cells were seeded into a confocal dish and incubated with PKH26-labeled BMP-TMZ or An-BMP-TMZ (TMZ concentration: 200 μM) for 1 h. After treatment, the cells were washed thrice with PBS and labeled with DAPI for 10 min. Confocal microscopy was performed to determine the results.

The specific uptake of An-BMP-TMZ by U87 and U251 cells was also assessed using flow cytometry. U87 and U251 cells were seeded into 6-well plates and treated with/without anti-LRP-1 antibody to block the LRP on glioma cells. After that, the cells were treated with PKH26-labeled BMP-TMZ or An-BMP-TMZ (TMZ concentration: 200 μM) for 1 h. Following this, the cells were washed with PBS and analyzed using flow cytometry.

The expression of LRP protein on U87 and U251 cells was determined with ELISA Kit (Fine Test) according to the manufacturer's instructions.

2.13. Cell apoptosis

To evaluate the potential cell apoptosis effect of An-BMP-TMZ on glioma cells, U87 and U251 cells were seeded into 6-well plates and treated with free TMZ, BMP-TMZ or An-BMP-TMZ (TMZ concentration: 200 μM) for 48 h. After treatment, the cells were stained using an Annexin V-FITC/PI Apoptosis Detection Kit (GENVIEW) following the manufacturer's instructions. Flow cytometry was used to determine the results.

2.14. Flow cytometry analysis of escaped nanoparticles from macrophages

CD47 serves as a crucial "don't eat me" signal to the innate immune system, and has been shown to protect nanoparticles from immune cell clearance. To investigate the role of CD47 in preventing monocyte-mediated clearance of nanoparticles, PKH26-labeled An-BMP-TMZ and CD47-blocked An-BMP-TMZ (achieved by incubation with excess anti-CD47 antibody) were incubated with 5×10^5 macrophages for 3 h at 37 °C. After treatment, the cells were washed with PBS and analyzed using flow cytometry.

2.15. Transport of An-BMP-TMZ across the in vitro BBB

To establish an *in vitro* BBB model, bEnd3 cells were seeded at a density of 1×10^5 cells into the upper chamber of transwells (0.4 μm polyester membrane, Sigma) [40]. U87 cells were plated in the bottom of 24-well plates at a density of 1×10^5 cells per well. After reaching confluency and forming monolayers, the integrity of the cell monolayer was assessed by measuring *trans*-endothelial electrical resistance (TEER) values. The model was deemed suitable for experimentation when TEER values exceeded 200 Ω/cm^2. PKH26-labeled BMP-TMZ or An-BMP-TMZ were then added to the upper chamber, and after 4 h of incubation, the amount of An-BMP-TMZ that crossed the membrane was measured using confocal microscopy.

2.16. LFU irradiation

All animal experiments were conducted following the approved animal protocol procedures by the Institutional Animal Care and Use Committee (IACUC) of Fujian Medical University. Animal behavior was closely monitored to minimize pain and suffering. Animals were euthanized in the event of significant deterioration in their health. To assess the impact of LFU irradiation on the ability of An-BMP-TMZ to cross the BBB in mice, balb/c female mice were assigned to five groups (n = 4 per group): control, BMP-TMZ, An-BMP-TMZ, BMP-TMZ with LFU irradiation and An-BMP-TMZ with LFU irradiation. Briefly, 50 μl/kg Optison (Molecular Biosystems, USA) was injected into the mice, and then EMS-9A model color diagnostic transcranial Doppler equipment (transducer diameter = 1.5 cm; frequency = 1 MHz; duration = 20 s, power = 12 mW; Shenzhen Delica Company, China) [41,42] was applied to the mice. One hour later, saline, PKH26 labeled BMP-TMZ and An-BMP-TMZ (TMZ dose = 20 mg/kg) were injected into the mice through the tail vein. Two hours after the injection, *in vivo* imaging system (AniView600, Biolight Biotechnology) was used to measure the amount of nanocarrier that crossed the BBB.

2.17. The biodistribution of an-BMP-TMZ

Balb/c female mice were divided into 5 groups: control, BMP-TMZ, An-BMP-TMZ, BMP-TMZ with LFU irradiation and An-BMP-TMZ with LFU irradiation. The relevant mice were operated according to the above LFU irradiation procedures. One hour later, PBS, PKH26-labeled BMP-TMZ, An-BMP-TMZ (TMZ dose = 20 mg/kg) were intravenously injected into mice. The organs were collected and determined with IVIS 2h later.

2.18. In vivo uptake of an-BMP-TMZ in glioma cells

We further determined the specific uptake of An-BMP-TMZ by glioma tumor cells. Mice were subjected to LFU irradiation, as described in the above procedures, followed by the injection of PKH67-labeled BMP-TMZ or An-BMP-TMZ (TMZ dose = 20 mg/kg) via tail vein injection. The brains of the mice were collected 2h later, fixed in a 10 % formalin solution. Then, the slides were deparaffinized, incubated in 3 % methanol-hydrogen peroxide, followed by incubation with anti-EGFR antibody (Alexa Fluor 555, red). The results were observed using a confocal microscope.

2.19. Safety study of an-BMP-TMZ in healthy mice

To assess the safety of An-BMP-TMZ to mice, mice were exposed to

LFU irradiation as described above and then respectively injected with 100 μL PBS (control), free TMZ (20 mg/kg), BMP-TMZ, or An-BMP-TMZ (TMZ dose = 20 mg/kg) every three days until day 21. At the end of the animal experiment, the blood samples and main organs (brain, heart, liver, spleen, lung, kidney) were collected. The organ section was stained by using H&E, and routine blood tests were conducted.

2.20. In vivo tumor inhibition

Female severely immunodeficient (C-NKG) mice [43] (5 weeks old, obtained from Cyagen Biosciences) were used to establish the Luci$^+$ U87 glioma model. Once the model was established, the mice were randomly divided into four groups: control, free TMZ, BMP-TMZ, and An-BMP-TMZ. All mice were exposed to LFU irradiation as described above and then respectively injected with 100 μL PBS (control), free TMZ (20 mg/kg), BMP-TMZ, or An-BMP-TMZ (TMZ dose = 20 mg/kg) every three days until day 21. IVIS were used to measure the size of tumors. The body weights of the mice were measured. And the brains were collected and stained with hematoxylin and eosin (H&E). To assess survival rate, animals were monitored daily up to the point of spontaneous death or approaching moribund status.

2.21. Statistical analysis

All data were presented as the mean ± SD. Student's t-test was used for statistical analysis of two groups, whereas differences among multiple groups were evaluated using one-way analysis of variance. The P value was calculated with the software GraphPad Prism 7. Significant differences are indicated as *$P < 0.05$, **$P < 0.01$, ***$P < 0.001$, and ****$P < 0.0001$. ns, not significant.

3. Results and discussion

3.1. Characterization of the nano-assembly

The preparation of the nano-assembly was carried out by self-assembly of mouse bone marrow-derived macrophage membranes, temozolomide and the targeted polymer (Fig. 1). Briefly, mouse bone marrow-derived macrophages were derived from BALB/c mice. The isolated BMDMs were lysed to remove its intracellular contents and the macrophages membranes were mixed with the targeted An-PEI, and then the mixture was physically extruded through an apparatus with 200-nm pores. The positive charge of An-PEI facilitated conjugation with the negatively charged macrophage membrane. The conjugation of An-PEI and the macrophage membrane resulted in a stable structure that neutralized the excess positive charge. Furthermore, the cell membrane coating on the nanoparticles' surfaces formed a diffusion barrier, effectively limiting the release of TMZ. The extracted BMDMs were characterized using bright field and flow cytometry, and F4/80 positive cells were counted (Fig. S1). The size distribution of the targeted nanocarrier (An-BMP-TMZ) and its control (BMP-TMZ) were determined using DLS (Fig. 2A–B), with hydrodynamic sizes of 174.9 ± 4.7 nm and 159.6 ± 1.6 nm, respectively. Atomic force microscopy (AFM) results showed sizes of 104 ± 7.2 nm and 95.7 ± 20.9 nm for BMP-TMZ and An-BMP-TMZ, respectively (Fig. 2C–D). Zeta-potential measurements were 9.5 ± 1.0 mV and 2.7 ± 0.2 mV (Fig. S2). The cationic polymer is advantageous to maintain the stability of the nanocarrier through electrostatic repulsion, and the excessive positive charge was shielded by the cell membrane to avoid the non-specific binding and unwanted cytotoxicity [44]. Transmission electron microscopy (TEM) revealed a round shape with good homogeneity in both BMP-TMZ and An-BMP-TMZ (Fig. 2E–F), which is consistent with previous literature that demonstrates the ability of encapsulating therapeutic payloads [19]. The BCA result showed that the conjugation efficiency of Angiopep-2 was 50.2 ± 4.8 %. The results indicate the successful formation of nanocarrier by combining macrophage membranes and targeted polymers. The coating of the cell membrane on the nanoparticles' surfaces formed a diffusion barrier, and limited the release of the TMZ.

Utilizing natural cell membranes as coatings for nanoparticles offers a promising approach to achieve the objectives of low toxicity, high biocompatibility, and to reduce immune clearance within complex *in vivo* environments. For example, the coating of polymeric nanoparticles with macrophage membranes has demonstrated effectiveness in immune evasion and homotypic targeting, which can be attributed to the presence of specific surface antigens, such as CD47, on the cell membranes [45,46]. CD47 is a "don't eat me" signal that is critical to the innate immune system, and the expression of CD47 on nanocarriers prevents their clearance by immune cells. We extracted proteins from
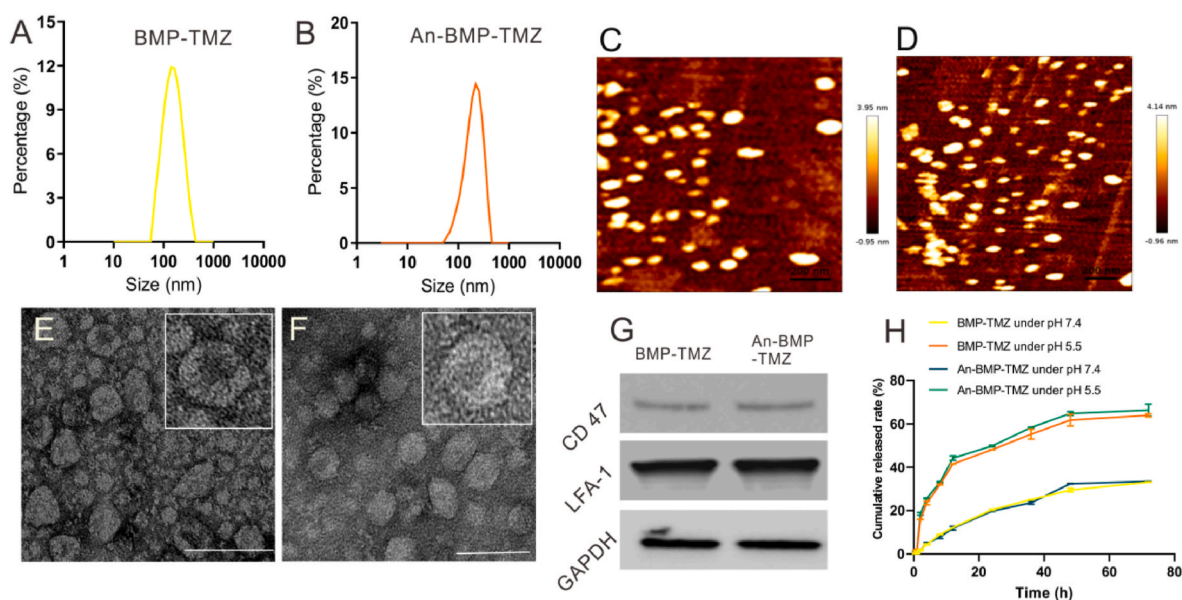

Fig. 2. The characterization of An-BMP-TMZ. (A–B) The size distribution of BMP-TMZ (A) and An-BMP-TMZ (B). (C–D) Representative AFM images of the BMP-TMZ (C) and An-BMP-TMZ (D). (E–F) Representative TEM images of the BMP-TMZ (E) and An-BMP-TMZ (F), scale bar = 100 nm. (G) Western blot analysis of the expression of CD47 and LFA-1 on BMP-TMZ and An-BMP-TMZ. (H) In vitro release of TMZ from BMP-TMZ and An-BMP-TMZ under pH 5.5 and pH 7.4.

BMP-TMZ, and An-BMP-TMZ and applied them to a western blot assay (Fig. 2G). Both cell membrane-coated nanocarriers expressed CD47 and LFA-1, suggesting a possible long circulation and the ability of crossing the endothelial barrier of BMP-TMZ and An-BMP-TMZ.

The macrophage membrane-coated nanoparticles described in this study share structural similarities with the widely studied lipid-polymer hybrid nanoparticles. These hybrid nanoparticles have gained attention as a promising multifunctional drug delivery platform, combining favorable characteristics of liposomes and polymeric nanoparticles [47–49]. Lipid-polymer hybrid nanoparticles have demonstrated a sustained drug release profile, attributed to the diffusional barrier provided by the lipid monolayer coating. Given the denser and bilayered lipid
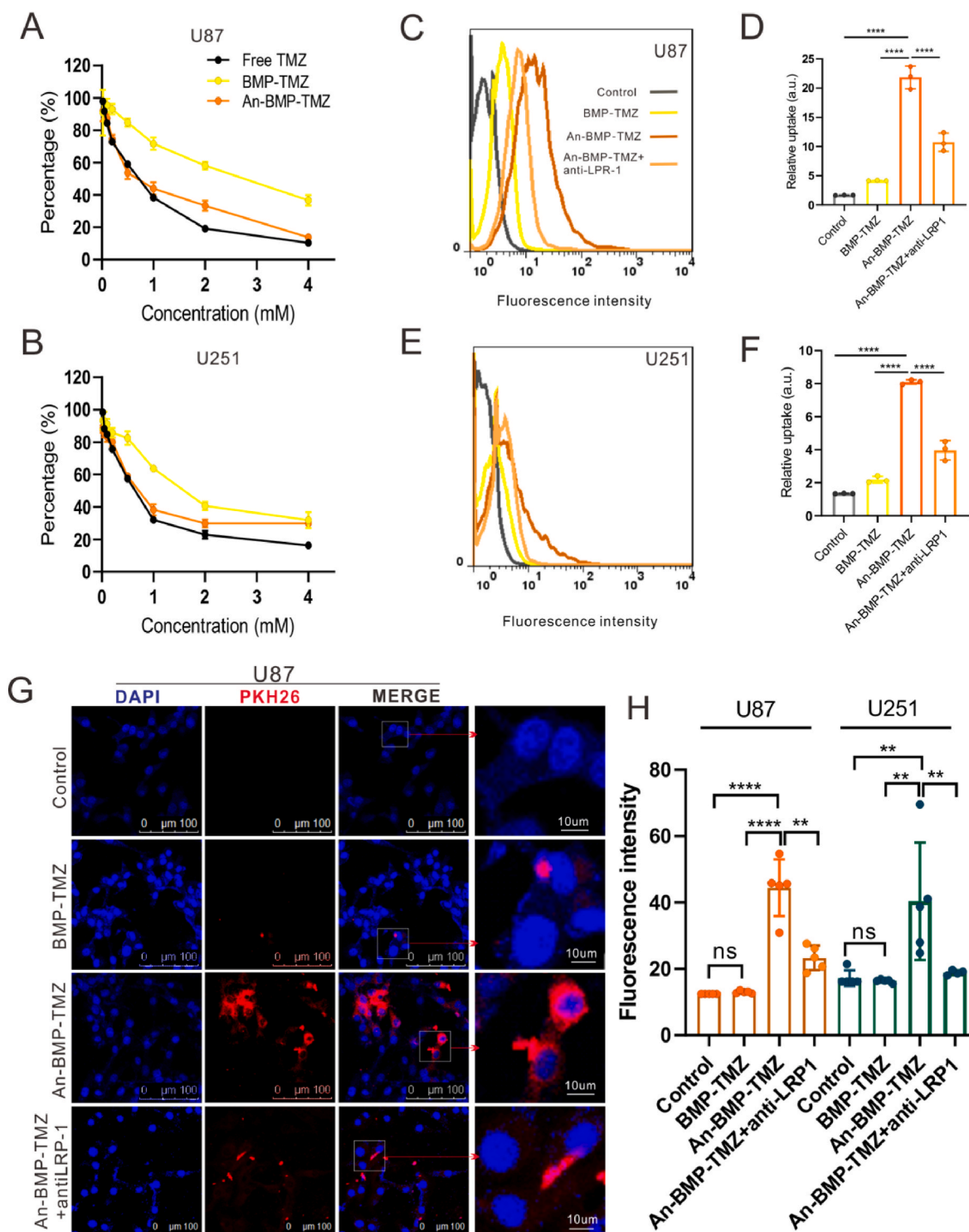

Fig. 3. The uptake of An-BMP-TMZ by glioma cells. (A–B) Viability of U87 and U251 cells after co-culture with different concentrations of free TMZ, BMP-TMZ or An-BMP-TMZ for 48 h. (C–F) Flow cytometry showing the uptake of BMP-TMZ or An-BMP-TMZ by U87 (C) and U251 (E) cells (with/without anti-LRP-1 blocking) after 1 h incubation, and the quantification (D, F). n = 3. (G–H) Confocal microscopy showing the uptake of BMP-TMZ and An-BMP-TMZ by U87 cells, and the quantification (H). n = 5. Data represent mean ± SD, and are statistically evaluated by one-way ANOVA. Significant differences are indicated as *P < 0.05, **P < 0.01, ***P < 0.001, and ****P < 0.0001. ns, not significant.

barrier offered by the macrophage membrane, the drug release kinetics from the macrophage membrane-coated nanoparticles is expected to be even more gradual. The amount of TMZ in the samples was determined by measuring absorbance at 330 nm, and we established a standard line between absorbance and TMZ concentration (Fig. S3). The cell membrane structure of the nanocarrier helping to retain the TMZ inside, and the encapsulation efficiency was 44.2 %. Considering the acidic environment in the tumor, we determined the release of TMZ from BMP-TMZ and An-BMP-TMZ under two different simulated pH conditions (pH 5.5 and pH 7.4). The release of TMZ from the BMP-TMZ and An-BMP-TMZ were rapidly raised at pH 5.5, while slowly at pH 7.4. After 72 h incubation, the accumulated release of TMZ from BMP-TMZ and An-BMP-TMZ reached 63.9 % and 66.4 % at pH 5.5 and 33.2 % and 33.5 % at pH 7.4 (Fig. 2H). The accelerated release of TMZ from An-BMP-TMZ at pH 5.5 and its decelerated release at pH 7.4 result from the protonation of PEI, resulting in enhanced release of therapeutic agents such as TMZ when the pH decreases to 5.5. This alteration leads to a significant drug release, potentially enhancing the accumulation of TMZ in tumors and minimizing its impact on normal tissues [50].

3.2. The stability of nanocarriers in mouse serum

The stability of nanocarriers is a critical factor for the success of targeted delivery. To assess stability, we employed a well-established absorbance method as described previously, to monitor the changes in particle size in the presence of mouse serum [6]. Monitoring the increase in size allows us to observe the aggregation of unstable particles. Therefore, An-BMP-TMZ were suspended in culture medium with 10 % FBS or mouse serum, and incubated for 4 h. The size distribution of An-BMP-TMZ did not change significantly in culture medium with 10 % FBS after 4 h of incubation, demonstrating the stability of the nanocarriers (Fig. S4). However, after incubation in mouse serum for 4 h, the particle size of the nanoparticles increased due to a large amount of protein in the serum forming a protein corona with the nanoparticles. Nevertheless, its size remained within an acceptable range (Fig. S5). Those properties provide the possibility for effective delivery of the nanocarriers to the tumor site in the brain.

3.3. In vitro cytotoxicity

The cytotoxicity of free TMZ, BMP-TMZ and An-BMP-TMZ in U87 and U251 cells was evaluated using an MTT assay after 48 h of incubation at various concentrations. Fig. 3A illustrates that at equivalent concentrations, An-BMP-TMZ exhibited significantly higher cytotoxicity towards U87 cells compared to BMP-TMZ. After 48 h of incubation with BMP-TMZ (containing 0.5 mM TMZ), the survival rate of U87 cells was 84.8 %, whereas for An-BMP-TMZ (containing 0.5 mM TMZ), it was 53.7 %. Similar results were observed in U251 cells, as shown in Fig. 3B. This enhanced cytotoxicity of An-BMP-TMZ may be attributed to the targeting ability of angiopep-2 towards the low-density lipoprotein receptor-related protein (LRP) on glioma cells [51]. To ensure the safety of the nanocarrier, both BMP and An-BMP underwent an *in vitro* cytotoxicity assay using the same PEI concentrations employed in the BMP-TMZ and An-BMP-TMZ formulations. The results were shown in Fig. S6. When the concentration of PEI was less than 38.8 μg/ml (equivalent to BMP-TMZ or An-BMP-TMZ containing 0.5 mM TMZ), nanocarriers showed no significant cytotoxicity. This finding demonstrates the safety of employing nanocarriers in this experiment.

3.4. In vitro uptake of nanocarriers

Previous studies have demonstrated that angiopep-2 exhibits targeting capabilities towards LRP on the BBB and glioma cells [51]. To investigate the specific recognition and uptake mediated by angiopep-2, PKH26-labeled BMP-TMZ and An-BMP-TMZ were incubated with U87 and U251 cells for 1 h, and the results were evaluated using flow cytometry and confocal microscopy.

Flow cytometry assays demonstrated that U87 cells exhibited a 15-fold and 5-fold increase in the uptake of An-BMP-TMZ compared to the control and BMP-TMZ, respectively (Fig. 3C–D). The uptake of An-BMP-TMZ by U251 cells showed a 5-fold and 4-fold increase compared to the control and BMP-TMZ, respectively (Fig. 3E–F). Moreover, after blocking with anti-LRP-1 antibody, the uptake of An-BMP-TMZ by U87 and U251 cells decreased obviously (Fig. 3C–F). These results can be attributed to the targeting ability of Angiopep-2 on An-BMP-TMZ to the LRP-1 on U87 and U251 cells (The expression of LRP-1 on U87 and U251 cells were shown in Fig. S7). Confocal microscopy images showed that U87 cells exhibited higher red fluorescence when incubated with PKH26-labeled An-BMP-TMZ compared to when incubated with PKH26-labeled BMP-TMZ (Fig. 3G–H). Similar result was founded in U251 cells. (Fig. S8). Consequently, An-BMP-TMZ demonstrates specific recognition of glioma cells, providing a promising approach for targeted treatment of glioma.

3.5. Escaping of nanocarriers from macrophages

The BBB-crossing efficiency is impaired by the rapid clearance of monocytes [52,53]. Membrane-modified drug delivery systems (DDS) incorporating natural proteins found on macrophages, such as CD47 and LFA-1, possess physical and chemical properties that contribute to immune evasion, prolonged circulation, and reduced toxicity (Fig. 4A). Above experiment proved the existence of CD47 on the macrophage membrane-coated nanoparticles (Fig. 2G). To investigate the role of CD47 in preventing nanoparticle clearance by monocytes, PKH26-labeled An-BMP-TMZ and CD47-blocked An-BMP-TMZ were incubated with macrophages. The results are presented in Fig. 4B–G, where the uptake of BMP-TMZ (Figs. 4C and 33.4 %) and An-BMP-TMZ (Figs. 4D and 50.5 %) significantly increased after blocking CD47 when compared with the unblocked groups (Fig. 4E–F, 17.3 % vs 29.9 %). This increase can be attributed to the presence of CD47 on unblocked nanocarriers, which prevents their clearance by macrophages. Interestingly, the escape efficiency between BMP-TMZ and An-BMP-TMZ is different, macrophages uptake more An-BMP-TMZ than BMP-TMZ. This difference may be due to the reduction of the positive charge of PEI by Angiopep-2 modification, resulting in a decrease of CD47 membrane coating. Conversely, the blocked nanocarriers are more readily cleared by macrophages. The natural proteins on An-BMP-TMZ enable efficient drug delivery to glioma cells in the brain.

3.6. Transport of nanocarriers across the BBB

The BBB is a significant hurdle that limits drug penetration into the brain, posing challenges in achieving optimal therapeutic effects for glioma-targeting drugs. Even if a drug exhibits good targeting efficacy against glioma, its therapeutic potential remains constrained by the BBB's limitations. To assess the BBB penetration ability of An-BMP-TMZ, we established an *in vitro* BBB model using bEnd3 cells (Fig. 5A). PKH26-labeled BMP-TMZ or An-BMP-TMZ were added to the upper chamber of the *in vitro* BBB model, in which bEnd3 cells were used to simulate the BBB structure. After 4 h of incubation, the amount of An-BMP-TMZ that crossed the membrane was measured using confocal microscopy. The transmembrane transport of An-BMP-TMZ by the U87 cells from the lower chamber was quantified and presented in Fig. 5B–C. Both BMP-TMZ and An-BMP-TMZ showed the ability to cross the *in vitro* BBB, with An-BMP-TMZ displaying notably higher transmembrane transport than BMP-TMZ. These results indicate that the coating of BMDMs membranes onto BMP-TMZ and An-BMP-TMZ is an effective strategy in enhancing BBB permeability of the drug delivery system (DDS). This effect may be attributed to the proteins present on the BMDMs cell membrane [33,54]. Furthermore, the angiopep-2 targeting group on An-BMP-TMZ further enhances its BBB crossing ability. These characteristics enable efficient delivery of TMZ to glioma in the brain via
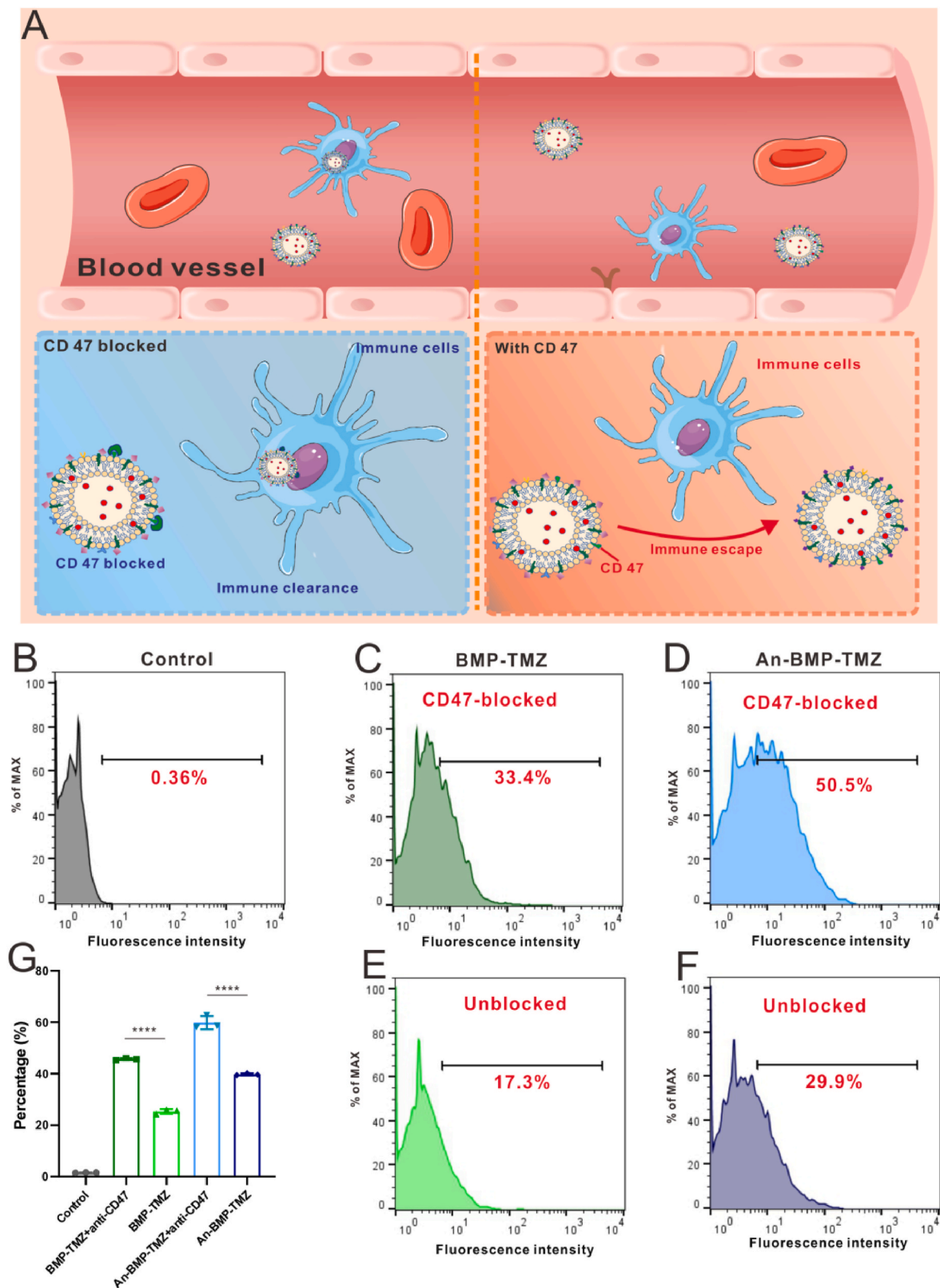
Fig. 4. Flow cytometry showing the uptake of BMP-TMZ and An-BMP-TMZ (with or without excess anti-CD47 antibody blocking) by macrophages after 3h incubation. (A) Schematic illustration of CD47 on An-BMP-TMZ prevents the immune clearance of An-BMP-TMZ by immune cells. (B) Control; (C) BMP-TMZ with anti-CD47 antibody blocking; (D) An-BMP-TMZ with anti-CD47 antibody blocking; (E) BMP-TMZ without anti-CD47 antibody blocking; (F) An-BMP-TMZ without anti-CD47 antibody blocking; (G) The quantification. Data represent mean ± SD, n = 3 and are statistically evaluated by one-way ANOVA. Significant differences are indicated as $*P < 0.05$, $**P < 0.01$, $***P < 0.001$, and $****P < 0.0001$. ns, not significant.
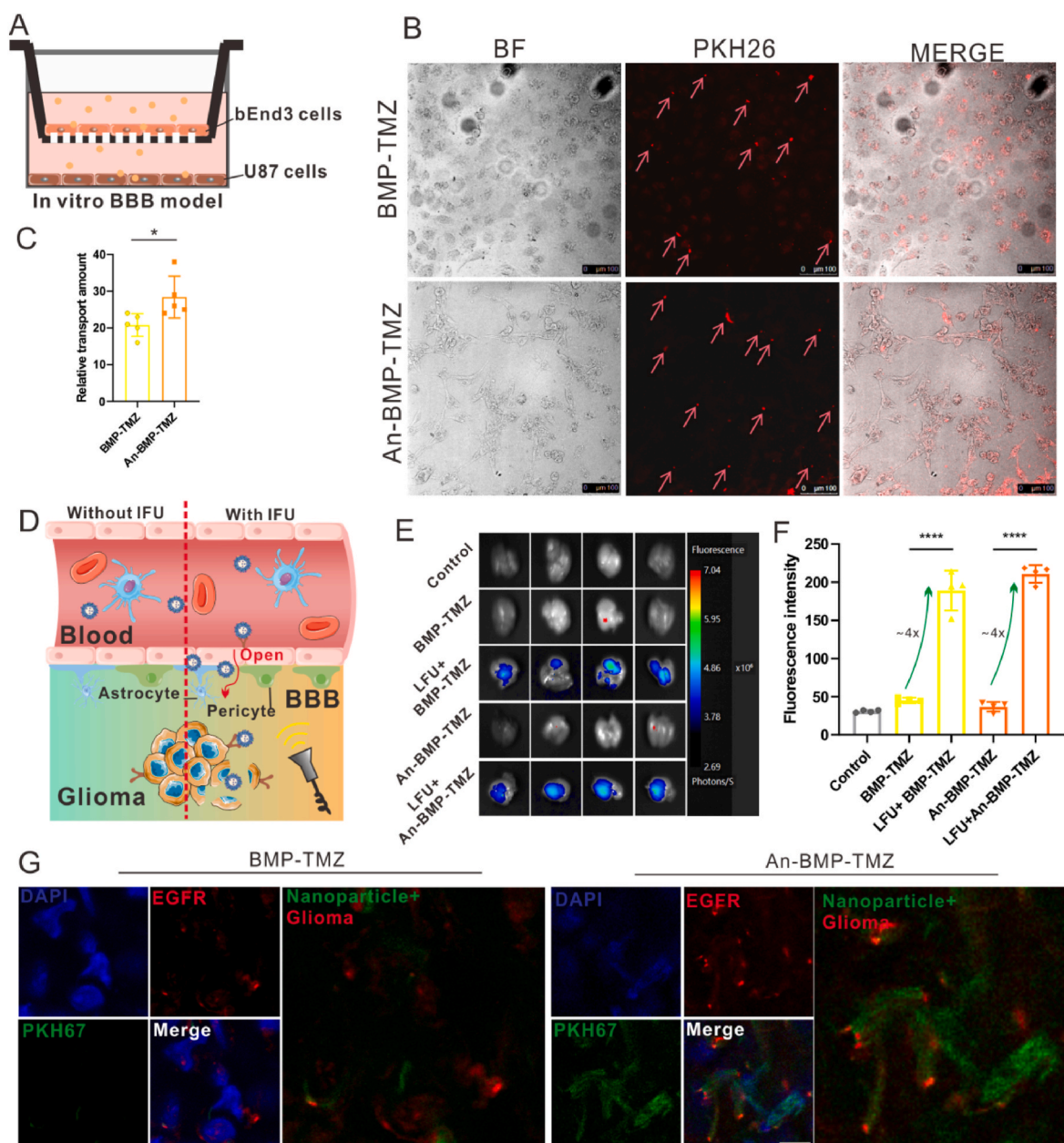
Fig. 5. Transport of An-BMP-TMZ across the In Vitro BBB. (A) Transwell model simulating *in vitro* BBB model. (B–C) Confocal microscopy showing nanoparticles crossing BBB monolayer. Red represents BMP-TMZ or An-BMP-TMZ (B) and the quantification (C). n = 5. (D) Illustration of LFU promoting nanoparticle to cross through BBB. (E–F) IVIS imaging showing the accumulation of An-BMP-TMZ in the brain of mice after i. v. injected with BMP-TMZ or An-BMP-TMZ (TMZ dose = 20 mg/kg) and treatment with/without LFU irradiation (E) and the quantification (F). n = 4. (G) Confocal microscopy showing the *in vivo* uptake of BMP-TMZ and An-BMP-TMZ in tumor (blue: DAPI, red: EGFR, green: PKH67). Scale bar = 10 μm. Data represent mean ± SD, and are statistically evaluated by one-way ANOVA. Significant differences are indicated as *P < 0.05, **P < 0.01, ***P < 0.001, and ****P < 0.0001. ns, not significant.

An-BMP-TMZ.

The effective penetration of the BBB for drug or gene delivery in GBM treatment has long been a challenge for researchers [55]. Recent breakthroughs in nanotechnology have resulted in versatile therapeutic nanoplatforms that possess the ability to cross the BBB, allowing for precise diagnosis and effective treatment of GBM. Our macrophage membrane-coated nanoparticles possess inherent advantages in terms of biocompatibility and their ability to penetrate the BBB, making them applicable in the field of brain diseases. However, despite their ability to penetrate the BBB, many researchers believe that intravenously injected biological nanomaterials are primarily distributed in the liver or spleen, with only a small fraction reaching the brain or tumor site [49]. Therefore, there is a need to develop a strategy for nanoparticles to

efficiently target glioma.

LFU irradiation has become widely utilized in nanocarriers across the BBB. The application of LFU irradiation, along with nanocarriers, offers a safe method for inducing BBB opening. This approach enables the efficient delivery of therapeutic group into the brain, enhancing its concentration and facilitating the treatment [36]. In this study, we introduced LFU irradiation to further improve the efficiency of drug delivery to tumors. We investigated the *in vivo* BBB transport of An-BMP-TMZ under the influence of LFU irradiation (Fig. 5D). Mice were subjected to LFU irradiation, followed by injection of saline, PKH26-labeled BMP-TMZ, or An-BMP-TMZ (TMZ dose = 20 mg/kg) via the tail vein. Imaging with IVIS was performed 1 h later to assess the amount of nanocarriers that crossed the BBB (Fig. 5E–F). *Ex vivo* images

revealed conspicuous fluorescence in the brains of LFU-irradiated mice treated with BMP-TMZ or An-BMP-TMZ, whereas no significant fluorescence was observed in the brains of mice treated only with BMP-TMZ or An-BMP-TMZ. This result may be result from the fact that without LFU treatment, the fluorescence of the nanocarrier passing through the BBB is obscured by the background, while with LFU treatment, the nanocarriers accumulate more in the brain, and the fluorescence becomes obvious. These results demonstrate that LFU irradiation promotes BBB permeability of BMP-TMZ or An-BMP-TMZ.

Since An-BMP-TMZ can efficiently cross the BBB under LFU irradiation, we further determined the specific uptake of An-BMP-TMZ by glioma tumor cells. Mice were subjected to LFU irradiation, followed by the injection of PKH67-labeled BMP-TMZ or An-BMP-TMZ via the tail vein injection. The brains of the mice were collected, and the glioma cells were labeled with anti-EGFR (red). The results were measured with a confocal microscope. As presented in Fig. 5G, more An-BMP-TMZ was

accumulated in glioma cells than BMP-TMZ. Moreover, the overlay of the nanoparticle (green) and glioma cells (red) demonstrated that the angiopep-2 on An-BMP-TMZ increased the specific recognition between An-BMP-TMZ and glioma cells.

In summary, the *in vitro* results proved that both BMP-TMZ and An-BMP-TMZ can traverse the BBB through the cell membrane on their surface, and the angiopep-2 modification further enhances BBB permeability. In the *in vivo* experiments, LFU irradiation treatment facilitates BBB opening, enabling more nanocarriers to enter the brain (~400 % increase). Additionally, the presence of angiopep-2 on An-BMP-TMZ enhanced specific recognition and mitigated potential side effects.

3.7. In vitro inhibition of glioma cells

Given their ability to cross the BBB and target gliomas, we decided to evaluate the inhibitory effect of An-BMP-TMZ on glioma cells. U87 and
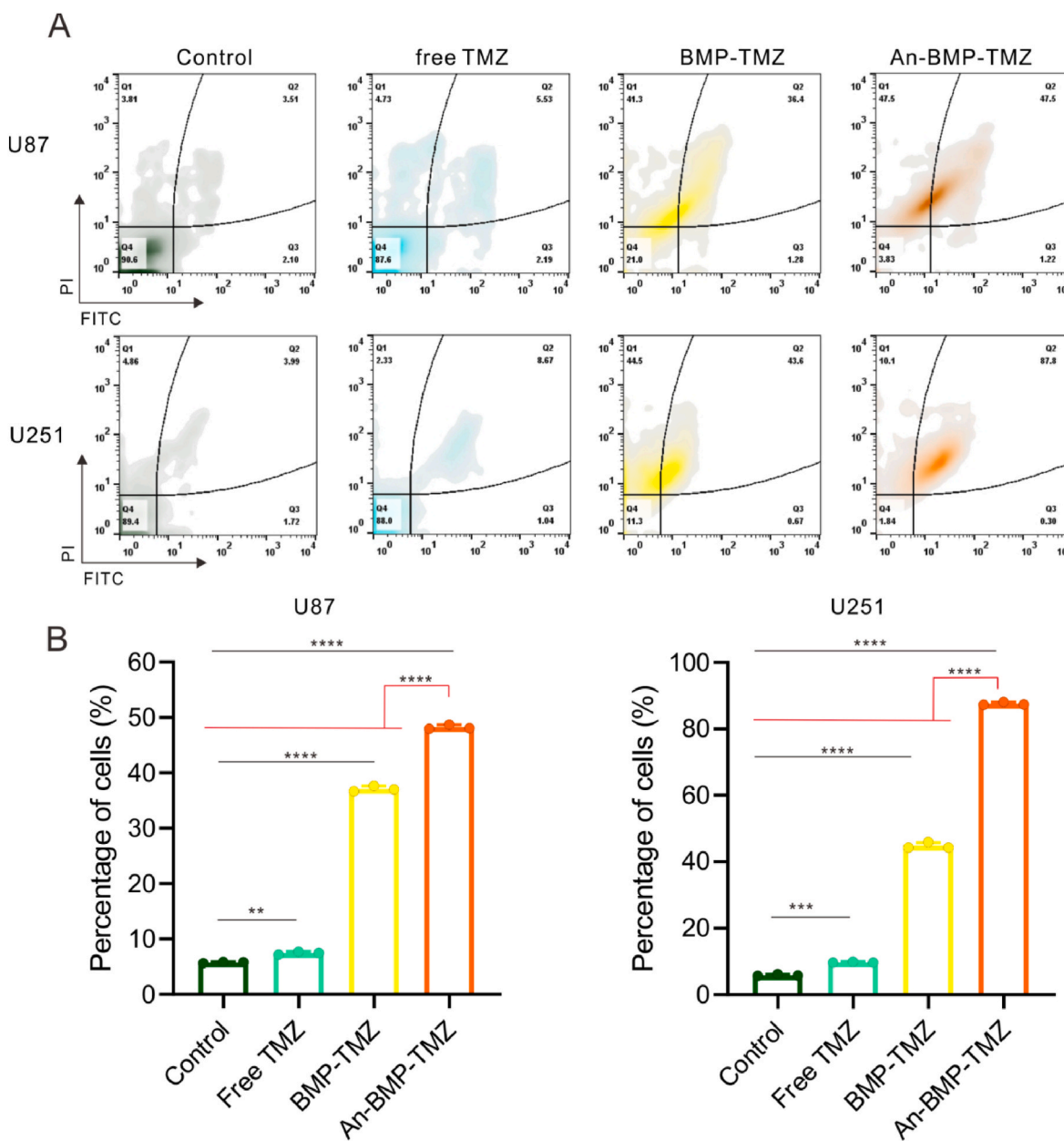

Fig. 6. In vitro apoptosis effect of An-BMP-TMZ on U87 and U251 cells. (A) Flow cytometry showing the apoptosis of U251 cells and U87 cells after treated with PBS, free TMZ, BMP-TMZ or An-BMP-TMZ for 48 h, and the quantification (B). Data represent mean ± SD, n = 3 and are statistically evaluated by one-way ANOVA. Significant differences are indicated as *P < 0.05, **P < 0.01, ***P < 0.001, and ****P < 0.0001. ns, not significant.

U251 cells were incubated with PBS, free TMZ, BMP-TMZ, and An-BMP-TMZ (TMZ concentration: 200 μM) at 37 °C for 48 h. After treatment, the cells were stained using the Annexin V-FITC/PI Apoptosis Detection Kit and analyzed by flow cytometry. As shown in Fig. 6A–B, the administration of An-BMP-TMZ significantly increased the percentage of apoptotic cells in U251 cells (73.5 %) compared to the BMP-TMZ (19.3 %), free TMZ (4.8 %), and control groups (8.5 %). Similar results were observed in U87 cells. The disparity between the An-BMP-TMZ and BMP-TMZ groups can be attributed to the presence of angiopep-2 on An-BMP-TMZ, which facilitated its uptake by U87 and U251 cells. These findings suggest that An-BMP-TMZ exhibits potent inhibition of glioma.

3.8. The biodistribution of an-BMP-TMZ

The biodistribution of nanocarriers following intravenous injection in mice has been extensively investigated by researchers. Previous studies reported that only a small portion of nanoparticles reach the brain or tumor site after intravenous injection into mice [56,57]. LFU irradiation-induced BBB-opening is regarded as a non-invasive, safe, and targeted approach for drug and gene delivery [36,58]. Nevertheless, the impact of LFU irradiation on the biodistribution of nanocarriers in extracerebral organs remains uncertain. To determine the effect of LFU irradiation on the biodistribution of An-BMP-TMZ, mice were first subjected to the LFU irradiation protocol described earlier, and 1 h later, PKH26-labeled BMP-TMZ and An-BMP-TMZ (TMZ dose = 20 mg/kg)
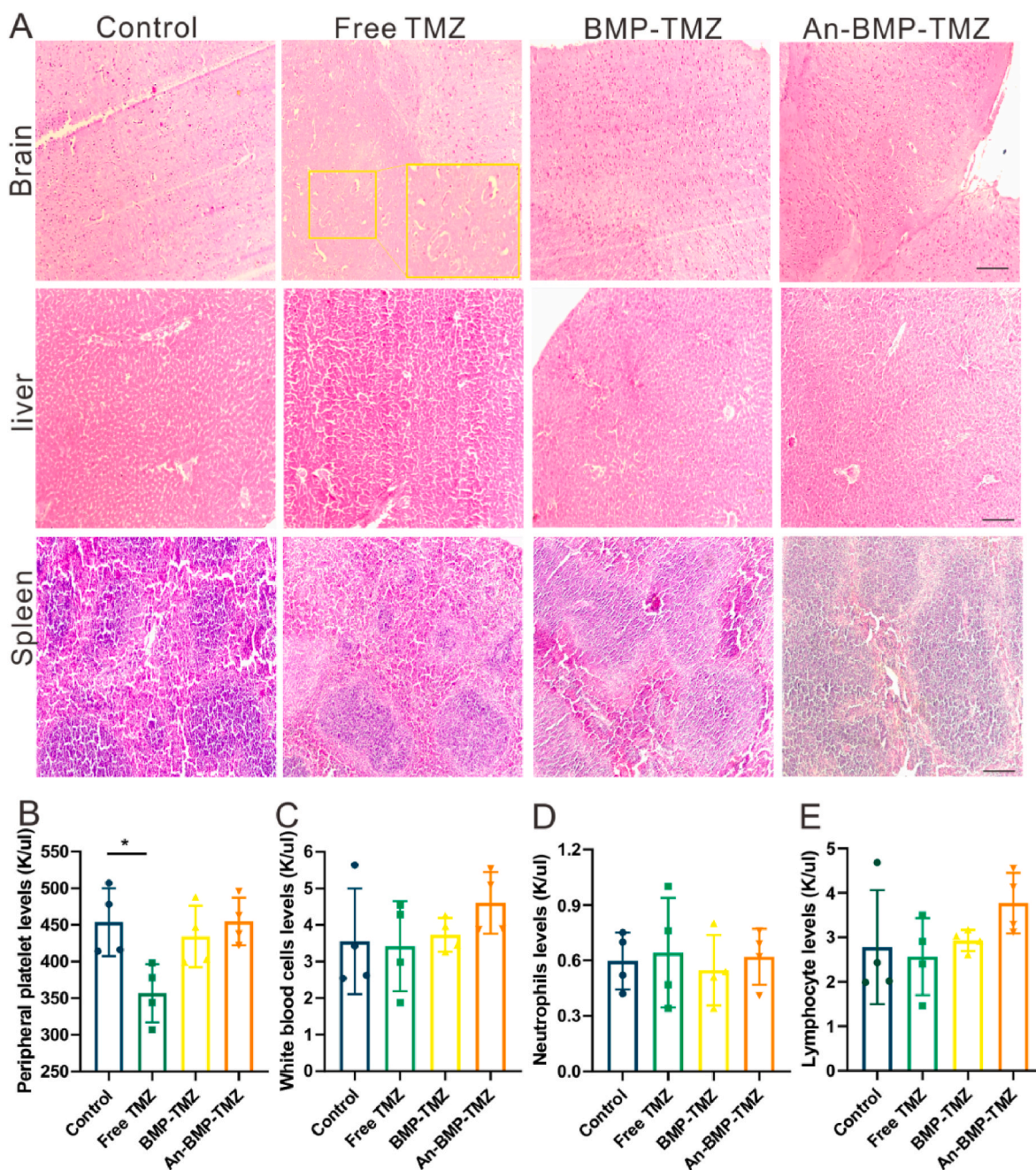

Fig. 7. *In vivo* safety of An-BMP-TMZ in healthy mice. (A) H&E staining of brain, liver, spleen in healthy mice after treated with PBS, free TMZ, BMP-TMZ and An-BMP-TMZ (Scale bar = 200 μm). (B–E) The platelet levels (B), white blood cells levels (C), neutrophils levels (D) and lymphocyte levels (E) in mice after treated with PBS, free TMZ, BMP-TMZ and An-BMP-TMZ. Data represent mean ± SD, n = 4 and are statistically evaluated by one-way ANOVA. Significant differences are indicated as *P < 0.05, **P < 0.01, ***P < 0.001, and ****P < 0.0001. ns, not significant.

were intravenously injected into the mice. The organs were collected and imaged using IVIS 2 h later. As shown in Fig. S9, in the absence of LFU irradiation treatment, BMP-TMZ and An-BMP-TMZ primarily accumulated in the lung and liver. However, after LFU treatment, there was an increased accumulation of BMP-TMZ and An-BMP-TMZ in the brain. These findings indicate that LFU can significantly enhance the accumulation of nanocarriers in the brain while reducing their accumulation in other organs, and mitigating associated side effects. This improvement in nanocarrier distribution enhances treatment efficacy while minimizing toxic side effects on normal organs.

3.9. In vivo toxicity evaluation

Toxic side effects contribute significantly to the failure of glioma chemotherapy, making the safety assessment of An-BMP-TMZ a crucial objective of this study. To mitigate these toxic side effects, mouse bone marrow-derived macrophage membranes were utilized to construct a nanocarrier with low toxicity and high biocompatibility. To determine the systemic toxicity of An-BMP-TMZ in mice, all mice were exposed to LFU irradiation and subsequently administered with PBS, free TMZ, BMP-TMZ, or An-BMP-TMZ every three days until day 21. Blood samples and major organs (brain, heart, liver, spleen, lung, kidney) were collected at the end of the animal experiment. As depicted in Fig. 7A and Fig. S10, organs treated with PBS, BMP-TMZ, and An-BMP-TMZ
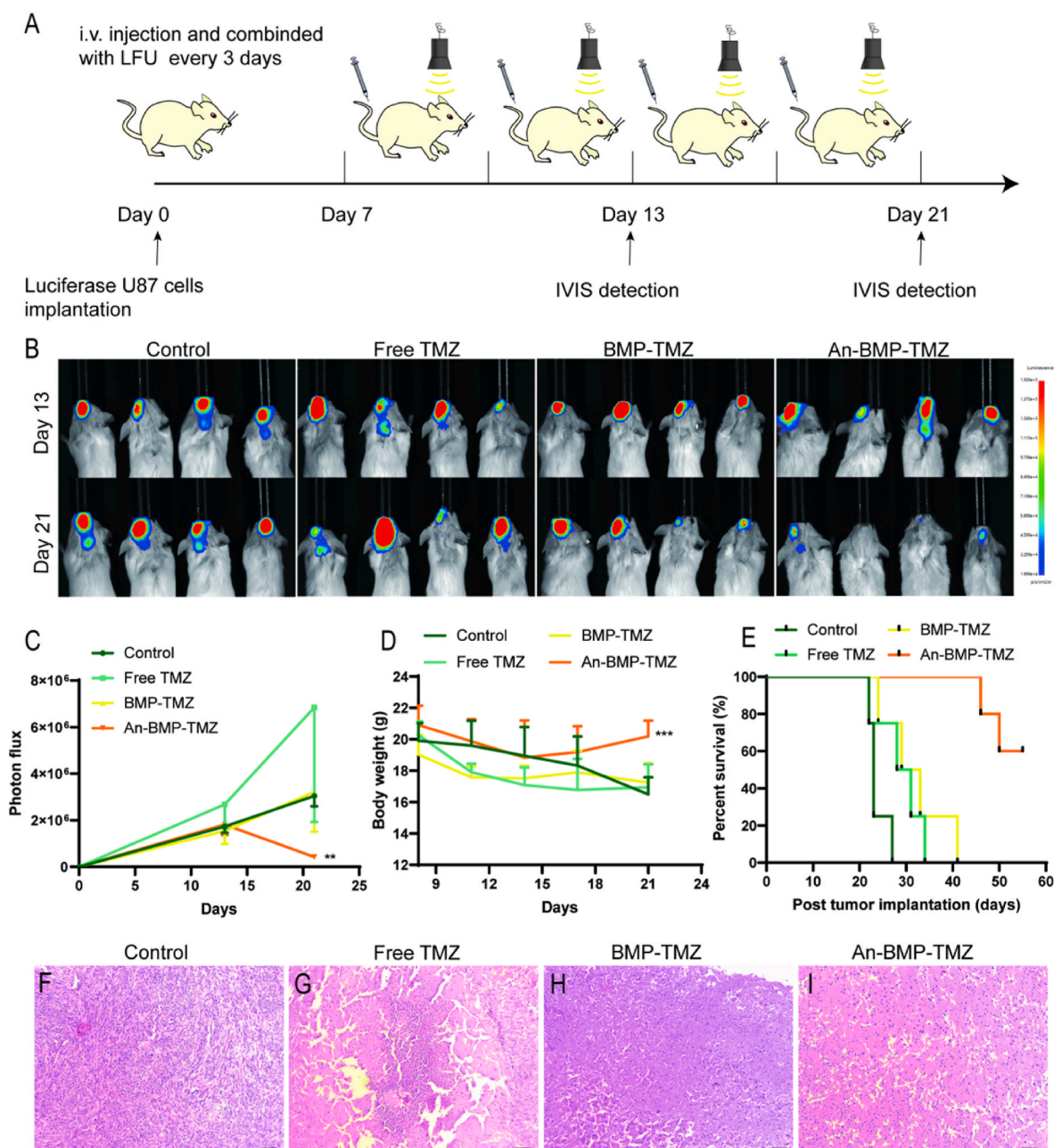

Fig. 8. Antitumor efficiency of An-BMP-TMZ. (A) The experimental scheme showing the treatment schedule. (B) Luminescence images of U87-Luc$^+$ tumor-bearing C-NKG mice following different treatments and monitored on days 13 and 21. (C) Quantitative analysis of the luminescence images. (D) Mouse body weight changes during different treatments. (E) Survival curves of the mice in the different groups. (F–I) The H&E staining images of brain of Control group (F), free TMZ group (G), BMP-TMZ group (H), An-BMP-TMZ (I), and scale bar = 200 μm. Data represent mean ± SD, n = 4 and are statistically evaluated by one-way ANOVA. Significant differences are indicated as *P < 0.05, **P < 0.01, ***P < 0.001, and ****P < 0.0001. ns, not significant.

exhibited no evident damage, indicating the favorable biocompatibility of BMP-TMZ and An-BMP-TMZ. However, treatment with free TMZ resulted in noticeable brain damage. Platelet levels, white blood cell levels, neutrophil levels, and lymphocyte levels in mice were also assessed (Fig. 7B–E). The findings revealed that treatment with free TMZ led to a significant decrease in blood platelet levels in mice. However, no noticeable changes were observed in platelet levels when treated with PBS, BMP-TMZ, and An-BMP-TMZ. These results demonstrated the safety and promising potential of *in vivo* application of BMP-TMZ and An-BMP-TMZ.

3.10. In vivo therapeutic studies

Since An-BMP-TMZ exhibits a prolonged circulation delivery profile, and LFU irradiation treatment and the targeting ability of An-BMP-TMZ can enhance the accumulation of An-BMP-TMZ in gliomas, we conducted a further evaluation of the antitumor effect of An-BMP-TMZ in a well-established GBM model. The GBM model was established using Luci$^+$ U87 cells to investigate the antitumor effects of the nanocarriers. Once the model was established, the mice were exposed to LFU irradiation and then administered with PBS, free TMZ, BMP-TMZ, or An-BMP-TMZ every three days until day 21 (Fig. 8A). Bioluminescence assays were used to measure tumor sizes. LFU irradiation combined with An-BMP-TMZ showed an inhibitory effect on tumor growth, as shown in Fig. 8B and the quantitative analysis (Fig. 8C). The tumor size in the An-BMP-TMZ group exhibited a significant decrease on day 21 compared to the control group, whereas the free TMZ and BMP-TMZ groups showed no noticeable changes. The body weights of the mice were monitored, and the results indicated that there was no significant difference between the free TMZ and BMP-TMZ groups compared to the control group, while the An-BMP-TMZ group showed a significant increase on day 21 (Fig. 8D). This may be attributed to LFU irradiation treatment significantly increased the accumulation of nanocarriers in the brain (Fig. 5E–F); moreover, the angiopep-2 on An-BMP-TMZ increased the specific uptake by tumor cells when compared to BMP-TMZ (Fig. 5G). The survival curve of the tumor-bearing mice showed that two mice treated with An-BMP-TMZ were still alive on day 55 (Fig. 8E). The We further evaluated the therapy effect of An-BMP-TMZ on inhibiting the glioma. As shown in Fig. 8F–I, the tumor burden in brains were confirmed by the H&E staining images. The An-BMP-TMZ group showed the best anti-cancer effect. These results indicate that the combination of this nanoplatform and LFU irradiation can efficiently penetrate the BBB, significantly inhibit glioma growth, and have no obvious side effects.

4. Conclusions

In summary, we have developed a promising nanocarrier by precisely controlling the self-assembly of the macrophage membrane, temozolomide, and the targeted polymer. With the intervention of LFU irradiation, the nano-assembly effectively crosses the BBB and accurately promotes apoptosis in glioma. Many studies have utilized LFU irradiation in combination with nanocarriers to facilitate drug delivery across the BBB, but most of these investigations have omitted consideration of the role of immune cells in the circulatory system regarding the clearance of nanocarriers. Furthermore, there is a tendency to ignore the potential toxicity of nanocarriers to normal brain tissue after crossing the BBB [34–36]. According to the results, there are several advantages of our nano-assembly. 1) The coating of the cell membrane created a diffusion barrier, which constrained the release of TMZ, and the release characteristics in acidic conditions may enhance TMZ accumulation in tumors while minimizing its impact on normal tissues. 2) The nanoparticle coated with the macrophage membrane, derived from mouse macrophages, exhibits excellent biocompatibility and safety. The presence of specific proteins, such as CD47, on the membrane of An-BMP-TMZ sends a "don't eat me" signal, thereby enhancing the circulation time of the An-BMP-TMZ. 3) The intervention of LFU

irradiation opened the BBB in mice and significantly enhanced the accumulation of An-BMP-TMZ in the mouse brain (up to 400 %). 4) Angiopep-2 peptide-modified An-BMP-TMZ exhibits the capability to penetrate the BBB and selectively target GBM cells after accumulation in the brain, resulting in effective suppression of primary brain tumor recurrence and prolongation of overall survival *in vivo*. 5) An-BMP-TMZ demonstrates excellent safety, attributed to its targeting ability and high biocompatibility derived from the coverage of mouse macrophage membrane, thereby avoiding toxic side effects. Our findings are expected to significantly contribute to the advancement of brain tumor treatment strategies, expanding the possibilities for precise treatment of brain tumors in the future.

Ethics approval and consent to participate

All animal experiments were conducted following the approved animal protocol procedures by the Institutional Animal Care and Use Committee (IACUC-FJMU 2023-Y-0905) of Fujian Medical University.

Availability of data and material

The data that support the findings of this study are available from the corresponding author upon reasonable request.

CRediT authorship contribution statement

Junqing Lin: Writing – original draft, Methodology, Conceptualization. **Zhenhu Lin:** Data curation. **Leilei Liu:** Investigation. **Wenjin Lin:** Investigation, Data curation. **Xiaodong Xie:** Writing – review & editing, Supervision, Resources, Methodology. **Xiujuan Zhang:** Writing – review & editing, Supervision, Methodology, Conceptualization.

Declaration of competing interest

The authors declare that they have no known competing financial interests or personal relationships that could have appeared to influence the work reported in this paper.

Data availability

Data will be made available on request.

Appendix A. Supplementary data

Supplementary data to this article can be found online at https://doi.org/10.1016/j.mtbio.2024.101067.

References

[1] M. Weller, W. Wick, K. Aldape, M. Brada, M. Berger, S.M. Pfister, R. Nishikawa, M. Rosenthal, P.Y. Wen, R. Stupp, G. Reifenberger, Glioma, Nat. Rev. Dis. Prim. 1 (2015) 15017.
[2] M. Xiao, C. Du, C. Zhang, X. Zhang, S. Li, D. Zhang, W. Jia, Bioinformatics analysis of the prognostic value of NEK8 and its effects on immune cell infiltration in glioma, J. Cell Mol. Med. 25 (2021) 8748–8763.
[3] G. Jia, Y. Han, Y. An, Y. Ding, C. He, X. Wang, Q. Tang, NRP-1 targeted and cargo-loaded exosomes facilitate simultaneous imaging and therapy of glioma in vitro and in vivo, Biomaterials 178 (2018) 302–316.
[4] H.V. Nguyen, V. Faivre, Targeted drug delivery therapies inspired by natural taxes, J. Contr. Release : official journal of the Controlled Release Society 322 (2020) 439–456.

[5] Z. Zhao, A. Ukidve, J. Kim, S. Mitragotri, Targeting strategies for tissue-specific drug delivery, Cell 181 (2020) 151–167.

[6] X. Xie, S. Lian, Y. Zhou, B. Li, Y. Lu, I. Yeung, L. Jia, Tumor-derived exosomes can specifically prevent cancer metastatic organotropism, J. Contr. Release : official journal of the Controlled Release Society 331 (2021) 404–415.

[7] M.D. Sweeney, A.P. Sagare, B.V. Zlokovic, Blood-brain barrier breakdown in Alzheimer disease and other neurodegenerative disorders, Nat. Rev. Neurol. 14 (2018) 133–150.

[8] W. Wang, Y. Zhang, Y. Jian, S. He, J. Liu, Y. Cheng, S. Zheng, Z. Qian, X. Gao, X. Wang, Sensitizing chemotherapy for glioma with fisetin mediated by a microenvironment-responsive nano-drug delivery system, Nanoscale 16 (2023) 97–109.

[9] N. McDannold, N. Vykhodtseva, K. Hynynen, Use of ultrasound pulses combined with Definity for targeted blood-brain barrier disruption: a feasibility study, Ultrasound Med. Biol. 33 (2007) 584–590.

[10] N. McDannold, N. Vykhodtseva, K. Hynynen, Targeted disruption of the blood-brain barrier with focused ultrasound: association with cavitation activity, Phys. Med. Biol. 51 (2006) 793–807.

[11] M. Reinhard, A. Hetzel, S. Kruger, S. Kretzer, J. Talazko, S. Ziyeh, J. Weber, T. Els, Blood-brain barrier disruption by low-frequency ultrasound, Stroke 37 (2006) 1546–1548.

[12] R. Stupp, W.P. Mason, M.J. van den Bent, M. Weller, B. Fisher, M.J. Taphoorn, K. Belanger, A.A. Brandes, C. Marosi, U. Bogdahn, J. Curschmann, R.C. Janzer, S. K. Ludwin, T. Gorlia, A. Allgeier, D. Lacombe, J.G. Cairncross, E. Eisenhauer, R. O. Mirimanoff, R. European Organisation for, T. Treatment of Cancer Brain, G. Radiotherapy, G. National Cancer Institute of Canada Clinical Trials, Radiotherapy plus concomitant and adjuvant temozolomide for glioblastoma, N. Engl. J. Med. 352 (2005) 987–996.

[13] P.S. Yasaswi, K. Shetty, K.S. Yadav, Temozolomide nano enabled medicine: promises made by the nanocarriers in glioblastoma therapy, J. Contr. Release : official journal of the Controlled Release Society 336 (2021) 549–571.

[14] M. Ismail, M. Yang, Y. Li, T. Chai, D. Zhang, Q. Du, P. Muhammad, S. Hanif, M. Zheng, B. Shi, Targeted liposomes for combined delivery of artesunate and temozolomide to resistant glioblastoma, Biomaterials 287 (2022) 121608.

[15] C. Hanna, K.M. Kurian, K. Williams, C. Watts, A. Jackson, R. Carruthers, K. Strathdee, G. Cruickshank, L. Dunn, S. Erridge, L. Godfrey, S. Jefferies, C. McBain, R. Sleigh, A. McCormick, M. Pittman, S. Halford, A.J. Chalmers, Pharmacokinetics, safety, and tolerability of olaparib and temozolomide for recurrent glioblastoma: results of the phase I OPARATIC trial, Neuro Oncol. 22 (2020) 1840–1850.

[16] B.C. Whitelaw, How and when to use temozolomide to treat aggressive pituitary tumours, Endocr. Relat. Cancer 26 (2019) R545–R552.

[17] R. Patil, J. Portilla-Arias, H. Ding, S. Inoue, B. Konda, J. Hu, K.A. Wawrowsky, P. K. Shin, K.L. Black, E. Holler, J.Y. Ljubimova, Temozolomide delivery to tumor cells by a multifunctional nano vehicle based on poly(beta-L-malic acid), Pharmaceut. Res. 27 (2010) 2317–2329.

[18] D.S. Pellosi, L.B. Paula, M.T. de Melo, A.C. Tedesco, Targeted and Synergic glioblastoma treatment: multifunctional nanoparticles delivering Verteporfin as adjuvant therapy for temozolomide chemotherapy, Mol. Pharm. 16 (2019) 1009–1024.

[19] R.H. Fang, C.M. Hu, B.T. Luk, W. Gao, J.A. Copp, Y. Tai, D.E. O'Connor, L. Zhang, Cancer cell membrane-coated nanoparticles for anticancer vaccination and drug delivery, Nano Lett. 14 (2014) 2181–2188.

[20] S. He, X. Gou, S. Zhang, X. Zhang, H. Huang, W. Wang, L. Yi, R. Zhang, Z. Duan, P. Zhou, Z. Qian, X. Gao, Nanodelivery systems as a novel strategy to Overcome treatment failure of cancer, Small Methods 8 (2024) e2301127.

[21] Y. He, Y. Ju, Y. Hu, B. Wang, S. Che, Y. Jian, W. Zhuo, X. Fu, Y. Cheng, S. Zheng, N. Huang, Z. Qian, J. Liu, P. Zhou, X. Gao, Brd4 proteolysis-targeting chimera nanoparticles sensitized colorectal cancer chemotherapy, J. Contr. Release : official journal of the Controlled Release Society 354 (2023) 155–166.

[22] J.W. Nichols, Y.H. Bae, EPR: Evidence and fallacy, J. Contr. Release : official journal of the Controlled Release Society 190 (2014) 451–464.

[23] L. Duan, L. Yang, J. Jin, F. Yang, D. Liu, K. Hu, Q. Wang, Y. Yue, N. Gu, Micro/nano-bubble-assisted ultrasound to enhance the EPR effect and potential theranostic applications, Theranostics 10 (2020) 462–483.

[24] R.H. Fang, W. Gao, L. Zhang, Targeting drugs to tumours using cell membrane-coated nanoparticles, Nat. Rev. Clin. Oncol. 20 (2023) 33–48.

[25] A. Narain, S. Asawa, V. Chhabria, Y. Patil-Sen, Cell membrane coated nanoparticles: next-generation therapeutics, Nanomedicine 12 (2017) 2677–2692.

[26] N. Krishnan, Y. Jiang, J. Zhou, A. Mohapatra, F.X. Peng, Y. Duan, M. Holay, S. Chekuri, Z. Guo, W. Gao, R.H. Fang, L. Zhang, A modular approach to enhancing cell membrane-coated nanoparticle functionality using genetic engineering, Nat. Nanotechnol. (2023).

[27] H. Sun, J. Su, Q. Meng, Q. Yin, L. Chen, W. Gu, P. Zhang, Z. Zhang, H. Yu, S. Wang, Y. Li, Cancer-cell-biomimetic nanoparticles for targeted therapy of homotypic tumors, Adv. Mater. 28 (2016) 9581–9588.

[28] W. Xie, W.W. Deng, M. Zan, L. Rao, G.T. Yu, D.M. Zhu, W.T. Wu, B. Chen, L.W. Ji, L. Chen, K. Liu, S.S. Guo, H.M. Huang, W.F. Zhang, X. Zhao, Y. Yuan, W. Dong, Z. J. Sun, W. Liu, Cancer cell membrane Camouflaged nanoparticles to Realize Starvation therapy Together with Checkpoint Blockades for enhancing cancer therapy, ACS Nano 13 (2019) 2849–2857.

[29] F. Zhou, B. Feng, H. Yu, D. Wang, T. Wang, Y. Ma, S. Wang, Y. Li, Tumor microenvironment-Activatable prodrug vesicles for Nanoenabled cancer Chemoimmunotherapy combining Immunogenic cell death Induction and CD47 blockade, Adv. Mater. 31 (2019) e1805888.

[30] H. Cao, Z. Dan, X. He, Z. Zhang, H. Yu, Q. Yin, Y. Li, Liposomes coated with isolated macrophage membrane can target lung Metastasis of Breast cancer, ACS Nano 10 (2016) 7738–7748.

[31] C.C. Ho, N. Guo, J.T. Sockolosky, A.M. Ring, K. Weiskopf, E. Ozkan, Y. Mori, I. L. Weissman, K.C. Garcia, "Velcro" engineering of high affinity CD47 ectodomain as signal regulatory protein alpha (SIRPalpha) antagonists that enhance antibody-dependent cellular phagocytosis, J. Biol. Chem. 290 (2015) 12650–12663.

[32] S. Lian, R. Xie, Y. Ye, X. Xie, S. Li, Y. Lu, B. Li, Y. Cheng, V.L. Katanaev, L. Jia, Simultaneous blocking of CD47 and PD-L1 increases innate and adaptive cancer immune responses and cytokine release, EBioMedicine 42 (2019) 281–295.

[33] D. Yuan, Y. Zhao, W.A. Banks, K.M. Bullock, M. Haney, E. Batrakova, A. V. Kabanov, Macrophage exosomes as natural nanocarriers for protein delivery to inflamed brain, Biomaterials 142 (2017) 1–12.

[34] L. Zhang, T. Yin, B. Li, R. Zheng, C. Qiu, K.S. Lam, Q. Zhang, X. Shuai, Size-modulable Nanoprobe for high-Performance ultrasound imaging and drug delivery against cancer, ACS Nano 12 (2018) 3449–3460.

[35] J. Wang, L. Xie, Y. Shi, L. Ao, F. Cai, F. Yan, Early Detection and reversal of cell apoptosis induced by focused ultrasound-mediated blood-brain barrier opening, ACS Nano 15 (2021) 14509–14521.

[36] Y. Shen, N. Li, S. Sun, L. Dong, Y. Wang, L. Chang, X. Zhang, F. Wang, Non-invasive, targeted, and non-viral ultrasound-mediated brain-derived neurotrophic factor plasmid delivery for treatment of autism in a rat model, Front. Neurosci. 16 (2022) 986571.

[37] W. Ying, P.S. Cheruku, F.W. Bazer, S.H. Safe, B. Zhou, Investigation of macrophage polarization using bone marrow derived macrophages, J. Vis. Exp. (2013).

[38] M. Tian, R. Xing, J. Guan, B. Yang, X. Zhao, J. Yang, C. Zhan, S. Zhang, A Nanoantidote Alleviates glioblastoma Chemotoxicity without efficacy Compromise, Nano Lett. 21 (2021) 5158–5166.

[39] X. Su, D. Zhang, H. Zhang, K. Zhao, W. Hou, Preparation and characterization of angiopep-2 functionalized Ginsenoside-Rg3 loaded nanoparticles and the effect on C6 Glioma cells, Pharmaceut. Dev. Technol. 25 (2020) 385–395.

[40] D. Liu, Y. Cheng, S. Qiao, M. Liu, Q. Ji, B.L. Zhang, Q.B. Mei, S. Zhou, Nano-codelivery of temozolomide and siPD-L1 to Reprogram the drug-resistant and Immunosuppressive microenvironment in Orthotopic glioblastoma, ACS Nano (2022).

[41] C.Y. Xia, Z. Zhang, Y.X. Xue, P. Wang, Y.H. Liu, Mechanisms of the increase in the permeability of the blood-tumor barrier obtained by combining low-frequency ultrasound irradiation with small-dose bradykinin, Journal of neuro-oncology 94 (2009) 41–50.

[42] N. McDannold, N. Vykhodtseva, K. Hynynen, Effects of acoustic parameters and ultrasound contrast agent dose on focused-ultrasound induced blood-brain barrier disruption, Ultrasound Med. Biol. 34 (2008) 930–937.

[43] H. Chen, L. Wu, T. Wang, F. Zhang, J. Song, J. Fu, X. Kong, J. Shi, PTT/PDT-induced microbial apoptosis and wound healing depend on immune activation and macrophage phenotype transformation, Acta Biomater. (2023).

[44] X. Xie, j. Jiang, X. Liu, Y. Cao, J. Li, T. Xia, H. Meng, Interleukin-10 plasmid delivery by polymeric nanocarrier shows efficient and safe tissue repair in acute muscle damage models in mice, Nano Today 46 (2022) 101544–101556.

[45] H. Xu, Y. Wang, X. Rong, D. Wang, J. Xie, Z. Huang, W. Zeng, X. Fu, J. Li, Z. Zhou, Ingenious Synergy of a Pathology-specific Biomimetic multifunctional nanoplatform for targeted therapy in Rheumatoid Arthritis, Small (2023) e2305197.

[46] T. Shen, S. Yang, X. Qu, Z. Chen, L. Zeng, X. Sun, Y. Lin, M. Luo, B. Lei, C. Yue, C. Ma, N. Hu, W. Wang, L. Zhang, A bionic "Trojan horse"-like gene delivery system hybridized with tumor and macrophage cell membrane for cancer therapy, J. Contr. Release : official journal of the Controlled Release Society 358 (2023) 204–218.

[47] S. Bou, X. Wang, N. Anton, R. Bouchaala, A.S. Klymchenko, M. Collot, Lipid-core/polymer-shell hybrid nanoparticles: synthesis and characterization by fluorescence labeling and electrophoresis, Soft Matter 16 (2020) 4173–4181.

[48] F. Li, H. Mei, Y. Gao, X. Xie, H. Nie, T. Li, H. Zhang, L. Jia, Co-delivery of oxygen and erlotinib by aptamer-modified liposomal complexes to reverse hypoxia-induced drug resistance in lung cancer, Biomaterials 145 (2017) 56–71.

[49] C. Liu, W. Zhang, Y. Li, J. Chang, F. Tian, F. Zhao, Y. Ma, J. Sun, Microfluidic sonication to Assemble exosome membrane-coated nanoparticles for immune evasion-mediated targeting, Nano Lett. 19 (2019) 7836–7844.

[50] W. Ma, Y. Yang, J. Zhu, W. Jia, T. Zhang, Z. Liu, X. Chen, Y. Lin, Biomimetic Nanoerythrosome-coated aptamer-DNA Tetrahedron/Maytansine Conjugates: pH-responsive and targeted cytotoxicity for HER2-positive Breast cancer, Adv. Mater. 34 (2022) e2109609.

[51] B. Li, X. Chen, W. Qiu, R. Zhao, J. Duan, S. Zhang, Z. Pan, S. Zhao, Q. Guo, Y. Qi, W. Wang, L. Deng, S. Ni, Y. Sang, H. Xue, H. Liu, G. Li, Synchronous Disintegration of Ferroptosis Defense Axis via Engineered Exosome-conjugated Magnetic nanoparticles for glioblastoma therapy, Adv. Sci. 9 (2022) e2105451.

[52] Z. Wang, M. Zhang, S. Chi, M. Zhu, C. Wang, Z. Liu, Brain tumor cell membrane-coated Lanthanide-Doped nanoparticles for NIR-IIb luminescence imaging and Surgical Navigation of glioma, Adv. Healthcare Mater. 11 (2022) e2200521.

[53] Z. Wang, E.D. Hood, J. Nong, J. Ding, O.A. Marcos-Contreras, P.M. Glassman, K. M. Rubey, M. Zaleski, C.L. Espy, D. Gullipali, T. Miwa, V.R. Muzykantov, W. C. Song, J.W. Myerson, J.S. Brenner, Combating Complement's Deleterious effects on Nanomedicine by conjugating Complement regulatory proteins to nanoparticles, Adv. Mater. 34 (2022) e2107070.

[54] R. Gorina, R. Lyck, D. Vestweber, B. Engelhardt, beta2 integrin-mediated crawling on endothelial ICAM-1 and ICAM-2 is a prerequisite for transcellular neutrophil diapedesis across the inflamed blood-brain barrier, J. Immunol. 192 (2014) 324–337.

[55] W. Tang, W. Fan, J. Lau, L. Deng, Z. Shen, X. Chen, Emerging blood-brain-barrier-crossing nanotechnology for brain cancer theranostics, Chem. Soc. Rev. 48 (2019) 2967–3014.

[56] Y. Gao, Y. Zhang, H. Xia, Y. Ren, H. Zhang, S. Huang, M. Li, Y. Wang, H. Li, H. Liu, Biomimetic virus-like mesoporous silica nanoparticles improved cellular internalization for co-delivery of antigen and agonist to enhance Tumor immunotherapy, Drug Deliv. 30 (2023) 2183814.

[57] S. Dong, X. Liu, Y. Bi, Y. Wang, A. Antony, D. Lee, K. Huntoon, S. Jeong, Y. Ma, X. Li, W. Deng, B.R. Schrank, A.J. Grippin, J. Ha, M. Kang, M. Chang, Y. Zhao,

R. Sun, X. Sun, J. Yang, J. Chen, S.K. Tang, L.J. Lee, A.S. Lee, L. Teng, S. Wang, L. Teng, B.Y.S. Kim, Z. Yang, W. Jiang, Adaptive design of mRNA-loaded extracellular vesicles for targeted immunotherapy of cancer, Nat. Commun. 14 (2023) 6610.

[58] K. Hynynen, N. McDannold, N. Vykhodtseva, F.A. Jolesz, Noninvasive MR imaging-guided focal opening of the blood-brain barrier in rabbits, Radiology 220 (2001) 640–646.